Simultaneous pulsating aurora and microburst observations with ground-based fast auroral imagers and CubeSat FIREBIRD-II

Miki Kawamura[1], Takeshi Sakanoi[1], Mizuki Fukizawa[1],
Yoshizumi Miyoshi[2], Keisuke Hosokawa[3], Fuminori Tsuchiya[1], Yuto Katoh[1],
Yasunobu Ogawa[4], Kazushi Asamura[5], Shinji Saito[6],
Harlan Spence[7], Arlo Johnson[9], Shin'ichiro Oyama[2,4,8], Urban Brändström[10]

1 Graduate School of Science, Tohoku University, Sendai, Japan
2 Institute for Space-Earth Environmental Research Nagoya University, Nagoya, Japan
3 The University of Electro-Communications, Chofu, Japan
4 National Institute of Polar Research, Tachikawa, Japan
5 Institute of Space and Astronautical Science, Japan Aerospace Exploration Agency, Sagamihara, Japan
6 NICT, Japan
7 Physics Department, University of New Hampshire, Durham, New Hampshire 03824, USA
8 University of Oulu, Pentti Kaiteran katu, Linnanmaa, Oulu, Finland
9 Physics Department, Montana State University, Bozeman, Montana 59717, USA
10 Swedish Institute of Space Physics, Kiruna, Sweden

Corresponding author: Miki Kawamura (kawamura@pparc.gp.tohoku.ac.jp)

Key Points:

- **We simultaneously identified a pulsating aurora and relativistic electron microburst for the first time**
- **We theoretically explain the detected time delay between a relativistic electron microburst and optical pulsation**
- **We confirm that relative to low-energy electron precipitations are commonly caused by chorus waves propagating along the same field line**

Abstract

We report on the relationship between pulsating aurora and relativistic electron microburst using simultaneous observations of ground-based fast auroral imagers with the FIREBIRD-II CubeSat for the first time. We conducted a detailed analysis of an event on October 8, 2018 and found that the occurrence of a pulsating aurora with internal modulations corresponds to the flux enhancement of electrons with energy ranging from 219.7 to 984.95 keV detected with Flight Unit 4, one of FIREBIRD's CubeSat, with a time delay of 525 ms. Assuming that the pulsating

aurora was produced by 10-keV electrons, we suggest that this time difference of 525 ms is consistent with the theory by Miyoshi et al. (2020) that a pulsating aurora and microburst occur due to the chorus waves at different latitudes along the same field line.

Plain Language Summary

It is thought that chorus waves generate low-energy electron precipitation that causes pulsating aurora and simultaneously generate a microburst, but there has been a lack of observational evidence. In this study, we detected a simultaneous pulsating aurora and microburst from coordinated ground-based and satellite observations for the first time. The velocity dispersion estimated in different energies matched the model curve. We suggest that the high-energy microburst and low-energy electron precipitation that cause a pulsating aurora are generated by chorus waves along the same magnetic field-line.

1 Introduction

A pulsating aurora is a type of diffuse aurora usually occurring on the morning side (Akasofu, 1968) and characterized by brightness modulation in both space and time. The modulating period of a pulsating aurora has a hierarchical structure. A few to a few-tens of second modulation is called the main pulsation, and a ~3-Hz modulation embedded within the main pulsation is called the internal modulation. A pulsating aurora is produced by the precipitation of magnetospheric electrons with energies ranging from a few to ~100 keV through pitch angle scattering due to the whistler-mode chorus waves near the magnetic equator (e.g., Sandahl et al., 1980, Miyoshi et al., 2010). Miyoshi et al. (2015a) proposed a model in which the main pulsations are caused by the pitch angle scattering with lower-band chorus (LBC) bursts, while the internal modulations are caused by the rising tone elements embedded in a single burst of an LBC. Direct evidence of the proposed model is obtained from the Arase satellite (Miyoshi et al., 2018) and ground-based observations (Hosokawa et al., 2020). Kasahara et al. (2018) investigated the electron flux inside the loss cone and confirmed that the pitch angle scattering due to an LBC causes the main modulation of a pulsating aurora. Hosokawa et al. (2020) confirmed that the internal modulations of a pulsating aurora are caused by the rising tone elements. Fukizawa et al. (2018, 2020) indicated that electrostatic cyclotron harmonic waves also contribute to a pulsating aurora. On the other hand, the upper-band chorus waves (Miyoshi et al., 2015a) cause background stable precipitations (Evans et al., 1987).

A microburst (about a few tens of keV) was first reported from X-ray emission fluctuations observed during a balloon experiment (Anderson and Milton,1964). A microburst is a periodic precipitation of sub-relativistic or relativistic electrons (Blake et al., 1996). Such highly energetic electrons in the range of a few MeV show a series of intermittent precipitations called “trains”. Previous studies suggested that such intermittent high-energy precipitations are caused by the pitch angle scattering with the whistler-mode chorus waves in the morning side (e.g., Brenemann et al., 2017), and with electromagnetic ion cyclotron waves in the dusk sector (e.g., Miyoshi et al., 2008, Blum et al., 2015).

Previous studies suggested that, in accordance with the variation in the first order cyclotron resonance condition along a field line, an LBC scatters electron, causing a pulsating aurora near the magnetic equator while resonating with sub-relativistic/relativistic electrons. This causes

78 microbursts in a region away from the magnetic equator (Miyoshi et al., 2010, Saito et al., 2012,
79 Miyoshi et al., 2015a). Miyoshi et al. (2010) also suggested that sub-relativistic to relativistic
80 electrons take longer time to reach the atmosphere from the modulation region. Therefore,
81 electrons arrive in the atmosphere in the order of middle energy electrons, sub-relativistic
82 electrons, and low-energy electrons. Miyoshi et al. (2020) proposed a hypothesis stating that
83 relativistic electron microbursts have the same origin as a pulsating aurora. That is, chorus waves
84 cause electron scattering in a wide energy range from a few keV to more than several MeV
85 simultaneously if the chorus waves can propagate to higher latitudes. Kurita et al. (2015)
86 conducted simultaneous observations of a diffuse aurora (non-pulsating) and precipitating
87 relativistic electrons using the data obtained from the SAMPEX satellite and an all-sky imager at
88 Syowa station, Antarctica. Miyoshi et al. (2015b) demonstrated that a few-hundred-keV
89 electrons precipitate into the mesosphere during a pulsating aurora, and the characteristics of
90 chorus waves simultaneously observed by Van Allen Probes well explain such wide-energy
91 electron precipitations. Grandin et al. (2017) and Tsuchiya et al. (2018) showed that tens-of-keV
92 electrons simultaneously precipitate into the upper atmosphere from ground-based observations.

93 Temporal variations of a pulsating aurora and microburst had not been compared directly in the
94 sub-second time scale. To reveal the relationship between these two sub-second-level
95 phenomena, we conducted simultaneous observations of these phenomena by combining high-
96 speed Electron Multiplying CCD (EMCCD) cameras in Scandinavia and observations from the
97 FIREBIRD satellite. We also clarified if the observed energy dispersion signature is consistent
98 with the model proposed by Miyoshi et al. (2020) by comparing with the theoretical time-of-
99 flight (TOF) model.

100 **2 Instruments**

101 To observe sub-second variations of a pulsating aurora, we used data from two all-sky EMCCD
102 imagers (ASIs) at Sodankylä (SOD) (67.37°N, 26.63°E in geographic coordinates) and Tjautjas
103 (TJA) (67.31°N, 20.73°E in geographic coordinates). The technical details of this system are
104 given by Hosokawa et al. (2021). The ASIs mainly capture auroral N_2^+ 1st negative-band
105 emission at 427.8 nm and N_2 1PG band emissions with the BG3 glass filter (Samara et al., 2012).
106 Both nitrogen emissions are called prompt emissions; thus, we do not need to consider any time
107 delay between the electron precipitation and optical emission. The frame rate is 100 Hz with a
108 time accuracy of ± 10 ms (Hosokawa et al., 2021), which is sufficiently high to detect ~3-Hz
109 internal modulations of a pulsating aurora.

110 FIREBIRD is a series of CubeSats missions (Johnson et al., 2020). The second mission of
111 FIREBIRD (FIREBIRD-II), which consists of Flight Unit 3 (FU3) and Flight Unit 4 (FU4), was
112 launched into 632-km apogee, 433-km perigee, and 99° inclination orbit on 31 January 2015
113 (Crew et al., 2016). We used the collimated detector on FU4 to observe electron fluxes in six
114 energy channels from ~220 keV to >1 MeV with a field-of-view of 54°. FIREBIRD-II's high-
115 resolution (HiRes) electron-flux data are gathered with an adjustable sampling period of 18.75
116 ms by default and can be as fast as 12.5 ms. FIREBIRD's time accuracy to the ground-
117 observation is ± 55 ms in the event of this paper. This error is calculated from a measurement
118 error and a time correction method error.

3 Observation and Results

We examined a conjunction event at SOD and TJA from ASIs and FU4 on October 8, 2018, during which the collimated detector on FU4 was operated with the HiRes mode at ~00:27:30 Universal Time (UT). This event occurred during the early recovery phase of a magnetic storm caused by a high-speed coronal hole stream. The Z component of the interplanetary magnetic field was large (from -15 to 10 nT) during the main phase, and the solar wind speed was still high (~600 km/s) during the recovery phase. The provisional AE index was ~700 nT. Pulsating aurorae appeared in the equatorward half of the fields-of-view of the ASIs after 23:50 UT on the previous day (around 3.4 magnetic local time (MLT)).

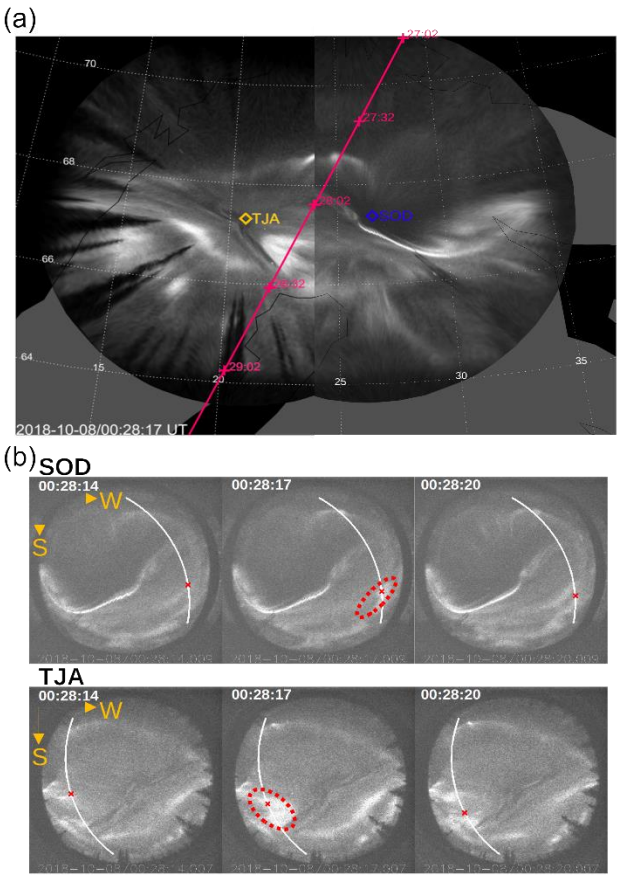

Figure 1. (a) Mosaic image of all-sky images captured at SOD and TJA at geographic coordinates at 00:28:17 UT on October 8, 2018. Red line indicates trajectory of FU4 from 00:27:02 to 00:29:32 UT. Mapped altitude was 90 km. (b) Successive all-sky images at SOD and TJA at intervals of 3 s from 00:28:14 to 00:28:20 UT on October 8, 2018. Solid line indicates trajectory of FU4, and red crosses indicates magnetic footprint of FU4. Dashed red circle is pulsating auroral patch we focused on in this study.

FU4 passed over the field-of-view of the ASIs at ~2.5 min intervals from 00:27:30 to 00:29:30 UT. During this period, FU4 was located at an altitude of ~525 km operated with Campaign 18, and the HiRes data were sampled at an interval of 50.0 ms. Figure 1a is a mosaic all-sky image obtained at SOD and TJA at 00:28:17 UT, where the trajectory of FU4 mapped at an altitude of 90 km in the geodetic coordinates is shown. This mapping altitude was chosen so that the pulsating aurorae in the two images smoothly connected. Although this altitude was relatively lower than the normal auroral height, past studies suggested that the altitude of a pulsating aurora is generally lower than that of a discrete aurora, and the current mapping altitude was probably in the range (Kataoka et al., 2013). The 13th International Geomagnetic Reference Field (IGRF) model (Alken et al., 2021) was used for tracing the location of FU4 along the field line.

We observed that FU4 passed over a pulsating aurora in the equatorward half of the field-of-view after ~ 00:28:02 UT. Figure 1b shows successive images from SOD and TJA with intervals of 3 s from 00:28:14 to 00:28:20 UT. This figure also shows a pulsating auroral patch from both SOD and TJA and a diffuse aurora around the patch. The FU4 footprint passed through the pulsating aurora patch at around 67.1°N, 23.1°E (L = 5.4). Animations are available as Movie S1 and S2 in the supporting information. In addition to the main pulsation with a period of ~2s, the internal modulation with a period of ~300 ms was clearly observed in the pulsating auroral patch in these animations.

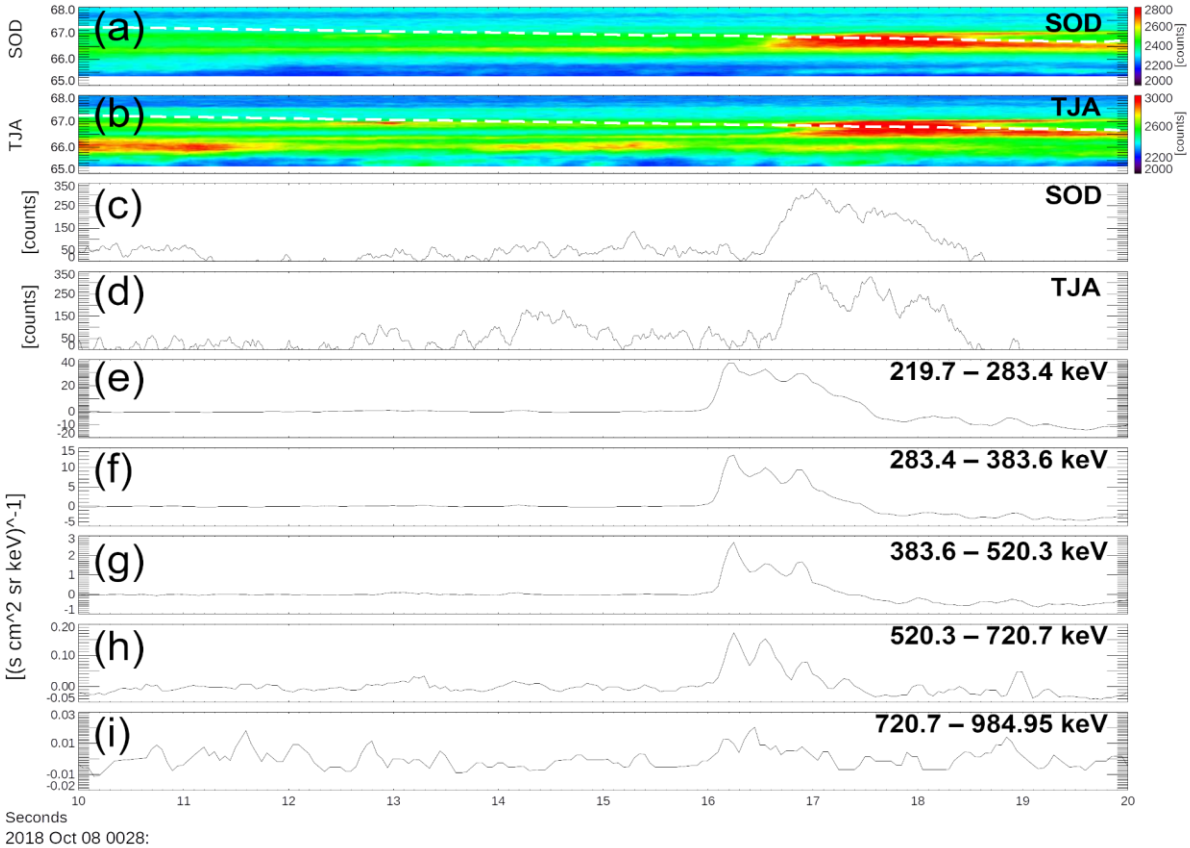

Figure 2. Summary plot of pulsating aurora and electron data from 00:28:10–00:28:20 UT on October 8, 2018. (a) and (b) Auroral emission counts at SOD and TJA, respectively. White dash line indicates trajectory of FU4. (c) and (d) Auroral intensities at SOD and TJA at locations of magnetic footprints of FU4. We plot relative variation by subtracting mean value for 3 s at each data point after averaging for 100 ms. (e) to (i) Electron energy fluxes in five energy channels at 219.7–283.4, 283.4–383.6, 383.6–520.3, 520.3–720.7, and 720.7–984.95 keV, respectively, obtained from FU4. In these panels, variation components are plotted from subtraction of mean value similar to (c) and (d).

Figure 2 shows the summary plot of optical and electron observations. Figures 2a and b indicate the auroral intensities at SOD and TJA, respectively, sampled along the geodetic north-south meridian including the instantaneous footprint of FU4. We focus on the pulsating auroral patch around 00:28:17 UT. Figures 2c and d show auroral intensities at the FU4 footprints with the field-of-view of SOD and TJA, respectively. Figures 2e−i show the precipitating electron fluxes at the five energy channels ranging from 219.7 to 984.95 keV obtained from the collimated detector with the HiRes mode of FU4. These data are the relative variation derived by subtracting a running average value (3-s window) after averaging for 100 ms. The electron fluxes enhanced at all the energy channels concurrently with the pulsating aurora at around 00:28:17 UT. The existence of sub-second modulation superimposed on the enhanced fluxes was also observed.

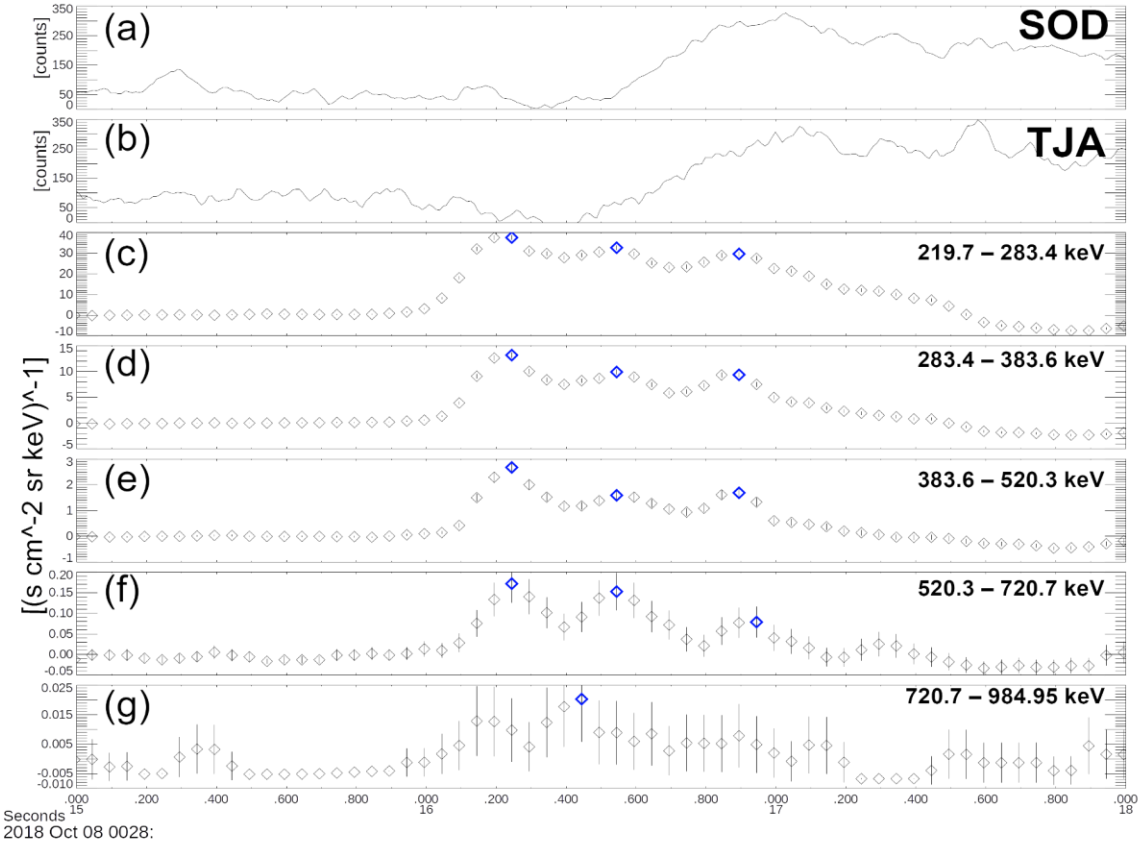

Figure3. Same as Figures 2(c) – (i) but expanded for 3 s from 00:28:16–00:28:19 UT. In each plot of electron flux, data with higher counts than surrounding data points and background data (observed from 00:28:12–00:28:15) is indicated in blue. Error bar is determined from square root of counts assuming random error.

We compared the timing of the electron-flux variation observed from FU4 with the variation of a pulsating aurora. Figures 3a and b show the variations of auroral intensities at the magnetic footprints of FU4 observed at SOD and TJA. Figures 3c–g show precipitating electron-flux data in the five energy ranges measured from FU4, and the peak flux is indicated in blue. The timing of pulsating auroral emission was observed 525 ms later than that of electron precipitations. Regarding the variations of electron fluxes, however, the time differences in the five energy channels were not clear. Therefore, we estimate the energy dispersion by comparing between the observed timing from FU4 and EMCCD camera and theoretical dispersion (Miyoshi et al., 2010, Saito et al.,2012) as described in the next section.

4 Discussion

We examined the difference in the timing of electron precipitation using the time-of-flight (TOF) model (Miyoshi et al, 2010, Saito et al., 2012). We found that the time difference between the high-energy precipitations obtained from FU4 and the pulsating auroral emission was 525 ms.

We assumed that the pulsating auroral emission was caused by electron precipitation at an energy of 10 keV, which is based on past rocket observations of a pulsating aurora, and precipitating electrons of several 10 of keV effectively cause ionization at an altitude of about 90 km (Sandahl et al., 1980, Rees, 1963).

We were not able to distinguish the time differences in the five energy channels of FU4 because of the insufficient time resolution of the detector (50.0 ms). To solve this problem, the timing difference between the channels was estimated from the instantaneous phase difference derived from electron-flux data using the Hilbert transform.

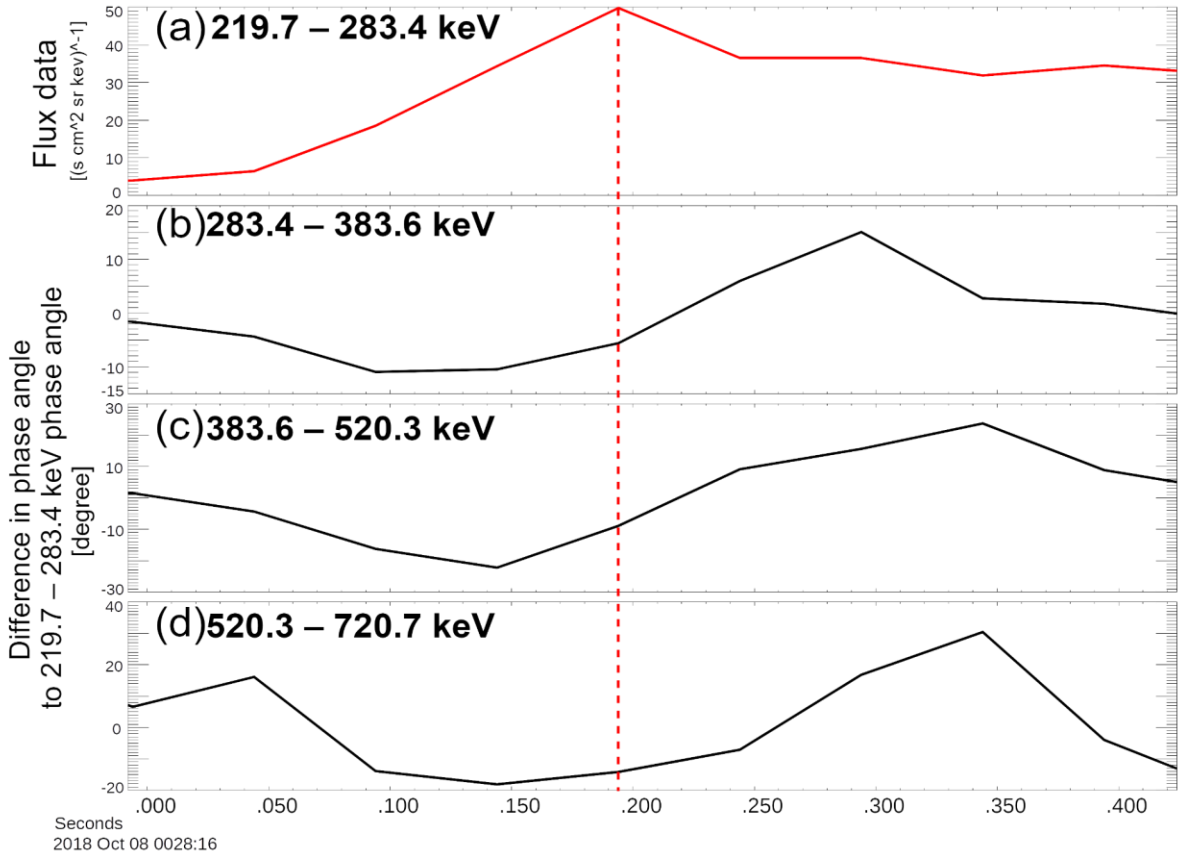

Figure 4. (a) Electron energy flux in energy range of 219.7–283.4 keV. (b) and (c) Differences in phase angle to phase angle in energy range of 219.7–283.4 keV calculated from Hilbert transform. Red dash line indicates peak point of electron energy flux in energy range of 219.7–283.4 keV.

Figure 4 shows the difference in the instantaneous phase differences derived by applying the Hilbert transform analysis to the data in three energy channels (from ~280 to ~ 720 keV). The time difference was calculated with respect to the time series of the ~220-keV channel. The data at 720.7–984.95 keV were not used because the noise level was high, as shown in

Figure 3. The Hilbert transform is given by

$$H(t) = \frac{1}{\pi} P \int_{-\infty}^{\infty} \frac{x(\tau)}{t-\tau} d\tau (1)$$

From the Hilbert transformation analysis, the phase differences of the three channels were 3.5, 6.0, and 26 degrees at a peak flux of ~220-keV electrons (see Figure 4). Negative phase differences indicate that that the peak of electrons at ~220 keV was observed earlier than ~280 to ~ 720 keV. The time delays of the three channels were derived as 8, 14, and 26 ms. In the process of calculating these delays, the angular frequency was determined from the instantaneous phase data of ~220 keV, assuming that all waves had the same frequency (7.4 rad/s). These results indicate that the timing of the precipitation of the ~ 280-keV electrons for 8 ms, ~ 383-keV electrons for 14 ms, and ~ 520 keV electrons for 26 ms was delayed with respect to the ~ 220-keV electron precipitation.

We calculated the TOF of precipitating electrons at L = 5.4 to explain the delays estimated above. The TOF model is used to take into account the wave-particle interactions with whistler-mode chorus waves propagating from the equator (Miyoshi et al., 2010, Saito et al., 2012). The resonant energy depends on the magnetic latitudes, so the pitch angle scattering of different energy electrons can occur continuously as the waves propagate toward a higher latitude along the field line. The model takes into account the energy-dependent path length and precipitation start time of the precipitating electrons, as well as the transit time of chorus waves. The resonant energy depends on the magnetic field intensity, whistler-wave frequency, and ambient electron density. In this TOF analysis, we assumed that the electron density is constant along the same field line and used a realistic magnetic field model. According to the TOF model, the propagation time of the wave increases at higher energy because the higher-energy electrons are scattered at higher magnetic latitudes in the opposite hemisphere. In addition, we considered about the sweep rate of chorus. We assume the sweep rate to 2 kHz in this TOF model, with reference to past research (Shue et al., 2015).

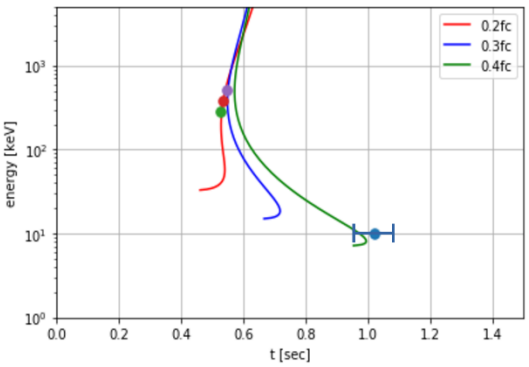

Figure 5. A result of TOF calculation at n = 7 /cc with f_{ceq} of 0.2 (red), 0.3 (blue), and 0.4 (green). Each dot is timing of peak of electron precipitations of 10, 219.7, 283.4, 383.6, and

520.3 keV. The error bar at the 10 keV electron precipitating timing is ± 65 ms considering from the time accuracy between FIREBIRD and EMCCD in this event.

Figure 5 shows the results of the TOF calculation and the fine timing of the peak of electron precipitation. We assumed that a pulsating aurora is generated by 10-keV electrons. Figure 5 shows the results with n of 7 /cc and f_{ceq} of 0.2 (red), 0.3 (blue), 0.4 (green) which are typical values on this L-shell (Sheeley et al., 2001). The error bar shows ± 65 ms considering of the relative time accuracy of FIREBIRD and EMCCD cameras.

During this event, we observed a pulsating aurora (~10-keV electrons) before the high-energy range electron precipitations (~220 keV). We also found positive energy dispersion in the energy range from ~220 to ~720 keV. These energy dispersions are consistent with the inverse dispersion of the TOF model in the point of the energy range and time scale. From this analysis, observed microburst is consistent with the TOF model (Miyoshi et al., 2010, Saito et al., 2012) in which propagating chorus waves cause the pitch angle scattering along the field line. Figure 5 considering the TOF model showed that sub-relativistic/relativistic electrons in the energy range from ~220 to ~720 keV precipitate into the upper atmosphere as observed by FU4.

The following two points should be discussed regarding the TOF analysis. First, there are several free parameters (electron density, whistler-wave frequency, and the launch timing of chorus) in this TOF analysis. We assume the ambient density from the empirical model (Sheeley et al., 2001) and typical lower-band chorus waves. Second, there are uncertainties in detecting the timing of electron precipitation from observation. The time accuracy of FIREBIRD and EMCCD to the Universal Time is ± 55 ms and ±10 ms respectively. Therefore, there exists uncertainty about the timing of EMCCD as shown in Figure 5, the TOF model using the assumed parameters reproduce overall trend of the observed energy dispersion by FU4 and EMCCD.

As shown in Figures 2c and d, we detected the internal modulations with a typical period of ~300 ms superimposed on the main pulsation. Interestingly, these modulations were also observed in the high-energy electrons obtained from FU4. This fact is consistent with the theory that the internal modulation of a pulsating aurora and relativistic electron microbursts are caused by the same rising tone proposed by Miyoshi et al. (2020). Miyoshi et al. (2020) argued that the propagation latitude of chorus waves is related to the highest energy of a microburst. Unfortunately, wave data are not available because there were no satellites at the same magnetic field line in this case. Further investigation is required to fully understand the latitudinal dependence of the energy range of precipitating electrons. In the future, Loss through Auroral Microburst Pulsations (LAMP) rocket campaign is planned to investigate the relationship between a pulsating aurora and microburst to clarify the spatiotemporal correspondence in more detail.

5 Conclusions

We found for the first time the simultaneous occurrence of a pulsating aurora and microburst on October 8, 2018. We observed modulations with a period of less than 1 s in both the pulsating auroral intensity and relativistic electron microbursts. The time difference between the electron precipitation and pulsating aurora was 525 ms. The time differences in the four energies from

~220 to ~ 720 keV were consistent with the model that takes into account scattering of electrons in a wide energy range by propagating chorus waves. This study confirms the theory that relativistic electron microbursts are the same product of pulsating aurora electrons caused by latitudinal-propagating chorus waves.

Acknowledgments, Samples, and Data

This work has been supported by JSPS KAKENHI JP 15H05747, 16H06286, 18H03727, 20H01959, 20H01955. The operation of the EMCCD camera at Sodankylä has been supported by Sodankylä Geophysical Observatory (SGO). The operation of the EMCCD camera at Tjautjas has been supported by Swedish Institute of Space Physics (IRF). The data files are obtained from the ERG Science Center operated by ISAS/JAXA and ISEE/Nagoya University (https://ergsc.nagoya-u.ac.jp, Miyoshi et al., 2018b). FIREBIRD data was made possible by the National Science Foundation grant numbers: 0838034, 1339414.

References

Akasofu, S. I. (1968). Polar and Magnetospheric Substorms. *Springer*, 22–31, 222–224.

Alken, P., Thébault, E., Beggan, C.D. et al. (2021). International Geomagnetic Reference Field: the thirteenth generation. Earth Planets Space 73, 49. https://doi.org/10.1186/s40623-020-01288-x

Anderson, K. A., & Milton, D. W. (1964). Balloon Observations of X Rays in the Auroral Zone 3. *Journal of Geophysical Research: Space Physics*, *69*(21).

Blake, J. B., Freden, S. C., & Paulikas, G. A. (1966). Precipitation of 400-kev electrons in the auroral zone. *Journal of Geophysical Research*, *71*(21), 5129–5134. https://doi.org/10.1029/jz071i021p05129" https://doi.org/10.1029/jz071i021p05129

Blum, L., Li, X., & Denton, M. (2015). Rapid MeV electron precipitation as observed by SAMPEX/HILT during high-speed stream-driven storms. *Journal of Geophysical Research: Space Physics*, 120, 3783–3794. https://doi.org/10.1002/2014JA020633

Breneman, A. W., Crew, A., Sample, J., Klumpar, D., Johnson, A., Agapitov, O., et al. (2017). Observations Directly Linking Relativistic Electron Microbursts to Whistler Mode Chorus: Van Allen Probes and FIREBIRD II. *Geophysical Research Letters*, *44*(22), 11,265-11,272. https://doi.org/10.1002/2017GL075001" https://doi.org/10.1002/2017GL075001

Crew, A. B., Spence, H. E., Blake, J. B., Klumpar, D. M., Larsen, B. A., O'Brien, T. P., et al. (2016). First multipoint in situ observations of electron microbursts: Initial results from the NSF FIREBIRD II mission. *Journal of Geophysical Research: Space Physics*, 121, 5272–5283.

Evans, D. S., G. T. Davidson, H. D. Voss, W. L. Imhof, J. Mobilia, and Y. T. Chiu. (1987). Interpretation of electron spectra in morningside pulsating aurorae, J. Geophys. Res., 92, 12,295–12,306, doi:10.1029/JA092iA11p12295

Fukizawa, M., Sakanoi, T., Miyoshi, Y., Hosokawa, K., Shiokawa, K., Katoh, Y., et al. (2018). Electrostatic Electron Cyclotron Harmonic Waves as a Candidate to Cause Pulsating Auroras. *Geophysical Research Letters*, *45*(23), 12,661-12,668. https://doi.org/10.1029/2018GL080145, https://doi.org/10.1029/2018GL080145

Fukizawa, M., Sakanoi, T., Miyoshi, Y., Kazama, Y., Katoh, Y., Kasahara, Y., et al. (2020). Pitch-angle scattering of inner magnetospheric electrons caused by ECH waves obtained with the Arase satellite. *Geophysical Research Letters*, 47, e2020GL089926. https://doi.org/10.1029/2020GL089926

Grandin, M., Kero, A., Partamies, N., McKay, D., Whiter, D., Kozlovsky, A., & Miyoshi, Y. (2017). Observation of pulsating aurora signatures in cosmic noise absorption data. *Geophysical Research Letters*, *44*(11), 5292–5300. https://doi.org/10.1002/2017GL073901

Hosokawa, K., Oyama, S., Ogawa, Y., Miyoshi, Y., Kurita, S., & Teramoto, M. (2021). A ground-based instrument suite for integrated high-time resolution measurements of pulsating aurora with Arase, 1–53.

Hosokawa, K., Miyoshi, Y., Ozaki, M., Oyama, S. I., Ogawa, Y., Kurita, S., et al. (2020). Multiple time-scale beats in aurora: precise orchestration via magnetospheric chorus waves. *Scientific Reports*, *10*(1), 3380. https://doi.org/10.1038/s41598-020-59642-8

Johnson, A. T., Shumko, M., Griffith, B., Klumpar, D. M., Sample, J., Springer, L., et al. (2020). The FIREBIRD-II CubeSat mission: Focused investigations of relativistic electron burst intensity, range, and dynamics. *Review of Scientific Instruments*, *91*(3). https://doi.org/10.1063/1.5137905

Kasahara, S., Miyoshi, Y., Yokota, S., Mitani, T., Kasahara, Y., Matsuda, S., et al. (2018). Pulsating aurora from electron scattering by chorus waves. *Nature*, *554*(7692), 337–340. https://doi.org/10.1038/nature25505

Kataoka, R., Miyoshi, Y., Shigematsu, K., Hampton, D., Mori, Y., Kubo, T., et al. (2013). Stereoscopic determination of all-sky altitude map of aurora using two ground-based Nikon DSLR cameras. *Annales Geophysicae*, *31*(9), 1543–1548. https://doi.org/10.5194/angeo-31-1543-2013

Kurita, S., Kadokura, A., Miyoshi, Y., Morioka, A., Sato, Y., & Misawa, H. (2015). Relativistic electron precipitations in association with diffuse aurora: Conjugate observation of SAMPEX and the all-sky TV camera at Syowa Station. *Geophysical Research Letters*, *42*(12), 4702–4708. https://doi.org/10.1002/2015GL064564

Miyoshi, Y., K. Sakaguchi, K. Shiokawa, D. Evans, J. Albert, M. Connors, and V. Jordanova (2008), Precipitation of radiation belt electrons by EMIC waves, observed from ground and space, Geophys. Res. Lett., 35, doi:10.1029/2008GL035727.

waves, J. Geophys. Res., 120, 7728-7736, doi:10.1002/2015JA021562

Miyoshi, Yoshizumi, Katoh, Y., Nishiyama, T., Sakanoi, T., Asamura, K., & Hirahara, M.

(2010). Time of flight analysis of pulsating aurora electrons, considering wave-particle interactions with propagating whistler mode waves. *Journal of Geophysical Research: Space Physics*, *115*(10), 1–7. https://doi.org/10.1029/2009JA015127" https://doi.org/10.1029/2009JA015127

Miyoshi, Y., S. Saito, K.Seki, T. Nishiyama, R. Kataoka, K. Asamura, Y. Katoh, Y. Ebihara, T. Sakanoi, M. Hirahara, S. Oyama, S. Kurita, and O. Santolik (2015a), Relation between energy spectra of pulsating aurora electrons and frequency spectra of whistler-mode chorus waves, J. Geophys. Res., 120, 7728-7736, doi:10.1002/2015JA021562

Miyoshi, Y., S. Oyama, S. Saito, H. Fujiwara, R. Kataoka, Y. Ebihara, C. Kletzing, G. Reeves, O. Santolik, M. Cliverd, C. Rodger, E. Turunen, and F. Tsuchiya. (2015b). Energetic electron precipitation associated with pulsating aurora: EISCAT and Van Allen Probes observations, J. Geophys. Res., 120, doi:10.1002/2014JA020690

Miyoshi Y, Shinohara I, Takashima T, Asamura K, Higashio N, Mitani T, Kasahara S, Yokota S, Kazama Y, Wang S-Y, Tam SW, Ho, P.T.P, Kasahara, Y, Kasaba Y, Yagitani S, Matsuoka A, Kojima H, Katoh H, Shiokawa K, Seki K. (2018). Geospace Exploration Project ERG, Earth Planets Space, 70:101, doi:10.1186/s40623-018-0862-0

Miyoshi, Y., K. Sakaguchi, K. Shiokawa, D. Evans, J. Albert, M. Conners, and V. Jordanova, Precipitation of radiation belt electrons by EMIC waves, observed from ground and space, Geophys. Res. Lett., 35, L23101, doi:10.1029/2008GL035727, 2008Miyoshi, Y., Saito, S., Kurita, S., Asamura, K., Hosokawa, K., Sakanoi, T., et al. (2020). Relativistic Electron Microbursts as High-Energy Tail of Pulsating Aurora Electrons. *Geophysical Research Letters*, *47*(21), 0–2. https://doi.org/10.1029/2020GL090360

Ress, M. H. (1963). Auroral ionization and excitation by incident energetic electrons. Planetary and Space Science, 11(10), 1209–1218. https://doi.org/10.1016/0032-0633(63)90252-6

Saito, S., Miyoshi, Y., & Seki, K. (2012). Relativistic electron microbursts associated with whistler chorus rising tone elements: GEMSIS-RBW simulations. *Journal of Geophysical Research: Space Physics*, *117*(10), 1–9. https://doi.org/10.1029/2012JA018020

Samara, M., Michell, R. G., & Hampton, D. L. (2012). BG3 Glass Filter Effects on Quantifying Rapidly Pulsating Auroral Structures. *Advances in Remote Sensing*, *01*(03), 53–57. https://doi.org/10.4236/ars.2012.13005

Sandahl, I., Eliasson, L. and Lundin, R. (1980). Rocket observations of precipitating electrons over a pulsating aurora. Geophys. Res. Lett., 7: 309-312. https://doi.org/10.1029/GL007i005p00309

Sheeley, B. W., Moldwin, M. B., Rassoul, H. K. & Anderson, R. R. (2001). An empirical plasmasphere and trough density model: CRRES observations. J. Geophys. Res. 106, 25631–25641

Shue, J.-H., Y.-K. Hsieh, S. W. Y. Tam,K.Wang,H.S.Fu,J.Bortnik,X.Tao,W.-C. Hsieh, and G. Pi (2015), Localtime distributions of repetitionperiods for rising tone lower bandchorus waves

in the magnetosphere,Geophys. Res. Lett., 42, 8294–8301,doi:10.1002/2015GL066107.

Tsuchiya, F., Hirai, A., Obara, T., Misawa, H., Kurita, S., Miyoshi, Y., et al. (2018). Energetic Electron Precipitation Associated With Pulsating Aurora Observed by VLF Radio Propagation During the Recovery Phase of a Substorm on 27 March 2017. *Geophysical Research Letters*, *45*(23), 12,651-12,660. https://doi.org/10.1029/2018GL080222